Human DNA methylation signatures differentiate persistent from resolving MRSA bacteremia

Yu-Ling Chang[a], Maura Rossetti[a], David W. Gjertson[a,b], Liudmilla Rubbi[c], Michael Thompson[c], Dennis J. Montoya[d], Marco Morselli[c], Felicia Ruffin[e], Alexander Hoffmann[f], Matteo Pellegrini[c], Vance G. Fowler Jr[e,1], Michael R. Yeaman[g,h,i,j,1], Elaine F. Reed[a,1,2], and with the MRSA Systems Immunology Group[3]

[a]Department of Pathology and Laboratory Medicine, David Geffen School of Medicine, University of California, Los Angeles, CA 90095; [b]Department of Biostatistics, Fielding School of Public Health, University of California, Los Angeles, CA 90095; [c]Department of Molecular Cell and Developmental Biology, University of California, Los Angeles, CA 90095; [d]School of Medicine, University of California, Davis, CA 95616; [e]Division of Infectious Diseases, Duke University, Durham, NC 27710; [f]Institute for Quantitative and Computational Biosciences, University of California, Los Angeles, CA 90095; [g]Division of Molecular Medicine, Harbor–University of California, Los Angeles Medical Center, Torrance, CA 90502; [h]Division of Infectious Diseases, Harbor–University of California, Los Angeles Medical Center, Torrance, CA 90502; [i]Lundquist Institute for Biomedical Innovation at Harbor–University of California, Los Angeles Medical Center, Torrance, CA 90502; and [j]Department of Medicine, David Geffen School of Medicine, University of California, Los Angeles, CA 90095

Edited by Lawrence Steinman, Stanford University School of Medicine, Stanford, CA, and approved December 21, 2020 (received for review January 15, 2020)

Persistent methicillin-resistant *Staphylococcus aureus* (MRSA) bacteremia is life threatening and occurs in up to 30% of MRSA bacteremia cases despite appropriate antimicrobial therapy. Isolates of MRSA that cause antibiotic-persistent methicillin-resistant *S. aureus* bacteremia (APMB) typically have in vitro antibiotic susceptibilities equivalent to those causing antibiotic-resolving methicillin-resistant *S. aureus* bacteremia (ARMB). Thus, persistence reflects host–pathogen interactions occurring uniquely in context of antibiotic therapy in vivo. However, host factors and mechanisms involved in APMB remain unclear. We compared DNA methylomes in circulating immune cells from patients experiencing APMB vs. ARMB. Overall, methylation signatures diverged in the distinct patient cohorts. Differentially methylated sites intensified proximate to transcription factor binding sites, primarily in enhancer regions. In APMB patients, significant hypomethylation was observed in binding sites for CCAAT enhancer binding protein-β (C/EBPβ) and signal transducer/activator of transcription 1 (STAT1). In contrast, hypomethylation in ARMB patients localized to glucocorticoid receptor and histone acetyltransferase p300 binding sites. These distinct methylation signatures were enriched in neutrophils and achieved a mean area under the curve of 0.85 when used to predict APMB using a classification model. These findings validated by targeted bisulfite sequencing (TBS-seq) differentiate epigenotypes in patients experiencing APMB vs. ARMB and suggest a risk stratification strategy for antibiotic persistence in patients treated for MRSA bacteremia.

Staphylococcus aureus | MRSA | persistence | epigenetics | DNA methylation

Persistent *Staphylococcus aureus* bacteremia (SAB) is serious, common, and potentially lethal (1), particularly when involving methicillin-resistant *S. aureus* (MRSA). Persistent SAB occurs when the infecting isolate is not cleared from the bloodstream, despite appropriate treatment with an antibiotic to which it exhibits susceptibility in vitro. However, mechanism(s) responsible for antibiotic-persistent methicillin-resistant *S. aureus* bacteremia (APMB) are incompletely understood (2–5). Recent studies have begun to explore specific host–pathogen interactions in APMB (6, 7). Bacterial, viral, and parasitic pathogens can directly and indirectly use cellular methylation machinery to preserve their survival and as such, can evade clearance by suppressing an effective host immune system (8). Our discovery that MRSA infection encodes innate immune memory supports the essential concept of epigenetic regulation of host defense against this organism (9, 10). Moreover, we recently reported that a g.25498283A > C polymorphism in DNA methyltransferase-3A (*DNMT3A*) differentiates patients experiencing persistent vs. resolving MRSA bacteremia outcomes (11). These findings support our hypothesis that distinct DNA methylomes exist in patients infected by MRSA and correspond to immunologic functions potentially shaping APMB vs. antibiotic-resolving methicillin-resistant *S. aureus* bacteremia (ARMB) outcomes.

DNA methylation plays a critical role in host immune regulation by contributing to innate or adaptive gene expression shaping molecular and cellular plasticity in immune response (12). Mechanistically, the classical understanding is that DNA hypomethylation at gene promoters enables gene transcription (13), whereas hypermethylation suppresses gene expression. Moreover, recent discoveries emphasize how unique DNA methylation patterns may correlate with specific

Significance

Up to 30% of methicillin-resistant *Staphylococcus aureus* (MRSA) bloodstream infections fail to resolve despite appropriate therapy. Such infections are persistent and life threatening. Because persistent MRSA isolates are susceptible to antibiotics in vitro, unique interactions among the pathogen, patient, and antibiotic occur in the body that lead to persistent outcomes. To study host factors involved in persistence, we used state-of-the-art methods to explore how genes are modified by methylation in patients who experience persistent vs. resolving MRSA bacteremia. Findings established distinct methylation patterns in these patients, including differential methylation signatures associated with important immune system and related genes. These results may enable approaches to identify and treat patients prone to persistent infection to improve therapeutic outcomes and save lives.

Author contributions: Y.-L.C., M.R., D.W.G., F.R., A.H., M.P., V.G.F., M.R.Y., and E.F.R. designed research; Y.-L.C., M.R., L.R., F.R., M.R.Y., and E.F.R. performed research; Y.-L.C., M.R., D.W.G., M.T., D.J.M., F.R., A.H., M.P., V.G.F., and E.F.R. contributed new reagents/analytic tools; Y.-L.C., D.W.G., M.T., D.J.M., M.M., M.P., and E.F.R. analyzed data; and Y.-L.C., M.R., D.W.G., M.P., V.G.F., M.R.Y., and E.F.R. wrote the paper.

Competing interest statement: V.G.F. reports grant/research support from MedImmune, Cerexa/Forest/Actavis/Allergan, Pfizer, Advanced Liquid Logics, Theravance, Novartis, Cubist/Merck, Medical Biosurfaces, Locus, Affinergy, Contrafect, Karius, Genentech, Regeneron, and Basilea; paid consultant for Pfizer, Novartis, Galderma, Novadigm, Durata, Debiopharm, Genentech, Achaogen, Affinium, Medicines Co., Cerexa, Tetraphase, Trius, MedImmune, Bayer, Theravance, Cubist, Basilea, Affinergy, Janssen, xBiotech, Contrafect, Regeneron, Basilea, and Destiny; membership with Merck as cochair for V710 vaccine; educational fees from Green Cross, Cubist, Cerexa, Durata, Theravance, and Debiopharm; and royalties from UpToDate. M.R.Y. is a founder and shareholder of NovaDigm Therapeutics, Inc., which develops vaccines and immunotherapeutics targeting multidrug-resistant pathogens, including *S. aureus*.

This article is a PNAS Direct Submission.

[1]V.G.F., M.R.Y., and E.F.R. contributed equally to this work.

[2]To whom correspondence may be addressed. Email: EReed@mednet.ucla.edu.

[3]A complete list of the MRSA Systems Immunobiology Group can be found in *SI Appendix*.

This article contains supporting information online at https://www.pnas.org/lookup/suppl/doi:10.1073/pnas.2000663118/-/DCSupplemental.

Published March 1, 2021.

disease subtypes and function as clinical indicators (12, 14). Likewise, bacterial infections are known to modify DNA methylation in host cells (15–17). Integrating these concepts, in the present study we analyzed methylome patterns by reduced representation bisulfite sequencing (RRBS) in well-characterized, optimally matched APMB and ARMB patient cohorts to explore our hypothesis that distinct DNA methylation signatures are associated with clinical APMB vs. ARMB outcomes. We then assessed whether differentially methylated sites (DMSs) localized to specific immune functions relevant to host defense against *S. aureus*. Next, we applied innovative methods to resolve specific immune cell subsets enriched in DMS associated with APMB vs. ARMB. Finally, we utilized targeted bisulfite sequencing (TBS-seq) to validate the differentially methylation signatures associated with APMB/ARMB outcomes.

Results

APMB and ARMB Cohorts Exhibit Distinct Demographic and Clinical Characteristics. The demographic and clinical variables of the study population are summarized in Table 1. APMB patients exhibited an increased incidence of death due to *S. aureus* infection (P = 0.04), a higher risk of metastatic infection ($P < 0.001$), and longer length of in-hospital stay ($P < 0.001$). In contrast, ARMB patients exhibited greater rates of cure (P = 0.01), neoplasm (P = 0.03), and recent surgeries (within 30 d prior to SAB; P = 0.02).

RRBS DNA Methylation Signatures Differ in APMB vs. ARMB Patients' Peripheral Blood. We utilized RRBS to determine if global methylation profiles distinguished APMB from ARMB. We then built a classification model based on the DNA methylation levels of all 749,212 5′-C-phosphate-G-3′ (CpG) sites using a logistic regression with elastic net regularization (18). The performance of the classification was evaluated by a 10-fold cross-validation of all the samples, and the average classification accuracy measured by a receiver operating characteristic (ROC) area under the curve (AUC) was 0.85 (Fig. 1*A*, blue bold line). This corresponds to a sensitivity of 75.7% and a specificity of 84.8% at the optimal cutoff, which maximized the sum of sensitivity and specificity. To contrast the classification performances with chance outcomes, we generated the ROC using randomly shuffled class labels (APMB and ARMB). As expected, AUC for the randomly shuffled class labels approximated 50% (Fig. 1*A*, black bold line). We then used methylkit (19) to identify methylation patterns associated specifically with APMB or ARMB. Methylation levels of 276 CpG DMSs were significantly associated with a persistent vs. resolving outcome (Fig. 1*B* and *SI Appendix*, Table S1). A total of 160 DMSs reflected relative hypomethylation and 116 DMSs exhibited hypermethylation in APMB compared with ARMB. Methylation patterns of the 276 DMSs encompassing 142 samples were then visualized (Fig. 1*C* and *SI Appendix*, Fig. S1). The hierarchical, agglomerative cluster analysis revealed an APMB cluster (left branch; containing 96.5% APMB samples) and an ARMB cluster

Table 1. Characteristics of study population

Characteristics	APMB, n = 70	ARMB, n = 72	P value*
Age, mean (median), y	61 (62)	61 (61)	0.74
Sex, male/female	38/32	42/30	0.74
Race, Caucasian/African American/unknown or others	32/36/2	34/36/2	0.95
Site of acquisition, hospital acquired/HCA community acquired/non-HCA community acquired	8/56/6	8/56/8	0.91
Source of bacteremia, endovascular infection/GI or GU infection/respiratory, lung or skin, soft tissue, joint/bone infection/unknown or none	23/12/3/19/13	18/11/7/22/14	0.67
Metastatic infection (abscess/arthritis/epidural abscess/meningitis/vertebral osteomyelitis/nonvertebral osteomyelitis/psoas abscess/septic emboli/septic thrombophlebitis/kidney abscess/endocarditis/others)	54 (12/10/5/0/8/9/5/15/8/1/27/4)	28 (9/2/2/0/1/7/2/3/4/2/5/3)	4.14e-06
APACHE II, mean (range)	18 (6–37)	16 (5–36)	0.16
LOS categories, <9/9–14/15–20/>20 d	9/19/19/23	28/22/11/11	9.75e-04
Type of procedures used to treat the infection			
Surgical removal of foreign device	33	16	2.55e-03
Surgical debridement	21	8	6.58e-03
Surgical insertion of foreign device	8	4	0.24
Abscess drainage	13	7	0.15
Other	33	34	1.00
Outcome, 90 d			
Cure	46	62	0.01
Recurrent SAB infection	12	5	0.07
Death due to SAB infection	10	3	0.04
Death due to other causes	2	2	1.00
Underlying comorbidity			
Neoplasm	7	18	0.03
Diabetic	37	42	0.61
Hemodialysis dependent	29	20	0.11
HIV positive	3	1	0.36
Transplant recipient	5	7	0.76
Injection drug use	1	1	1.00
Corticosteroid use, 30 d	16	16	1.00
Surgery past 30 d	11	24	0.02

For metastatic infection, some patients have more than one type of metastatic infection. APACHE II, Acute Physiology and Chronic Health Evaluation II; GI or GU, gastrointestinal or genitourinary; HCA, health care associated; LOS, length of stay.
*The t test was used for continuous variables; the Fisher's exact test was used for categorical variables.

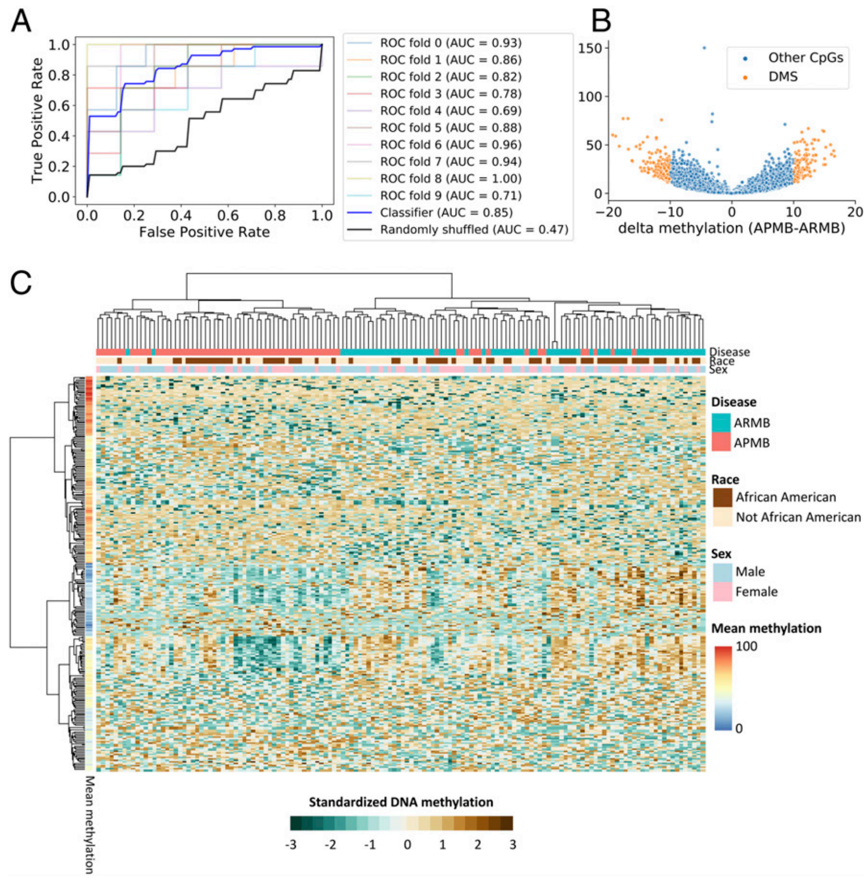

Fig. 1. Peripheral blood leukocyte DNA methylation is altered in patients with APMB. (*A*) ROC curve summarizes the test set classification performance (estimated by 10-fold cross-validation) of a logistic regression model that uses the DNA methylation levels of 749,212 CpG sites to distinguish APMB and ARMB samples. (*B*) Volcano plot represents the methylation difference for 749,212 CpG by delta methylation (percentage) and –log10 adjusted *P* value (FDR) generated from methylkit. The cutoff to define DMS (orange dots) was set as FDR < 0.01 and |delta methylation| > 10%. (*C*) The heat map displays DNA methylation for DMS (row) across all SAB samples (column). The clusters were generated using the sex-, race-, and batch-corrected DNA methylation data with Ward.D2 method shown in *SI Appendix*, Fig. S1. Keeping the same clustering order shown in *SI Appendix*, Fig. S1, the standardized DNA methylation (*z* score) was applied to visualize the relative methylation differences in this figure.

(right branch; containing 82.4% ARMB samples). The algorithm also clustered DMSs into two major groups consisting of 131 DMSs in cluster 1 (comparatively hypermethylated; mean methylation levels, 46.8 to 87.3%) or 145 DMSs in cluster 2 (comparatively hypomethylated; mean methylation levels, 16 to 64.6%).

To further investigate the differential methylation profiles focusing on sequence elements containing more than one CpG site (two or more CpG sites per region), CpG sites were clustered into 126,144 regions using the dynamic fragments method in CGmapTools (20). A classification model was then used to construct the 126,144 regions. The average AUC generated from 10-fold cross-validation using true class labeling was 0.88 (*SI Appendix*, Fig. S2*A*), with a sensitivity of 0.81 and a specificity of 0.85 at the optimal threshold. There were six CpG regions significantly associated with an APMB vs. ARMB outcome based on the methylkit analysis (*SI Appendix*, Fig. S2*B* and Table S3). All six of these differentially methylated regions (DMRs) were captured with at least one CpG site in the 276 identified DMSs. Together, these data reveal significant methylation signature differences in patients experiencing APMB vs. ARMB outcomes.

Specific DMSs Prioritize Differential APMB vs. ARMB Signatures in a Classification Model. To evaluate and rank DMSs based on their discrimination power to identify APMB, we used the 276 DMSs to build a logistic regression model with elastic net regularization. A wrapper method (21) was used to iteratively concentrate the parsimonious subsets of DMSs with high absolute model coefficients and censor DMSs with low discriminating capability. Box plots summarize the results of this process by reporting AUC generated from each iteration (Fig. 2*A*). Average AUC with true labels systematically increased, as DMSs with high discriminating ability were concentrated, and peaked when including 16 specific DMSs. We contrasted the DMS performances with chance outcomes by calculating the AUC for randomly permuted class labels (APMB and ARMB), which approximated 50%, as expected. Next, we evaluated the classification performance of the top 16-ranked DMSs by 10-fold cross-validation. The average AUC for the classifiers built based on the DNA methylation levels of the top 16-ranked DMSs was 0.98 (Fig. 2*B*), corresponding to a sensitivity of 91.4% and a specificity of 98.9% at the optimal cutoff. By calculating the odds ratio using the model coefficients, nine DMSs (odds ratio > 1) were positively associated with APMB, while another seven DMSs (odds ratio < 1) were negatively associated with APMB (Fig. 2*C*). Thus, even with the degree of overfitting, these data suggest that DNA methylation profiles can aid in or even predict APMB classification, given methods of our unbiased classifier in which DMSs were selected based on all the samples.

DMSs Are Enriched in Introns and Intergenic Regions. Next, we investigated the immunological relevance of the principal 276 DMSs identified. First, we explored whether the DMSs localized to promoter regions with potential to directly regulate gene transcription. Here, distances between a target DMS and the transcription start

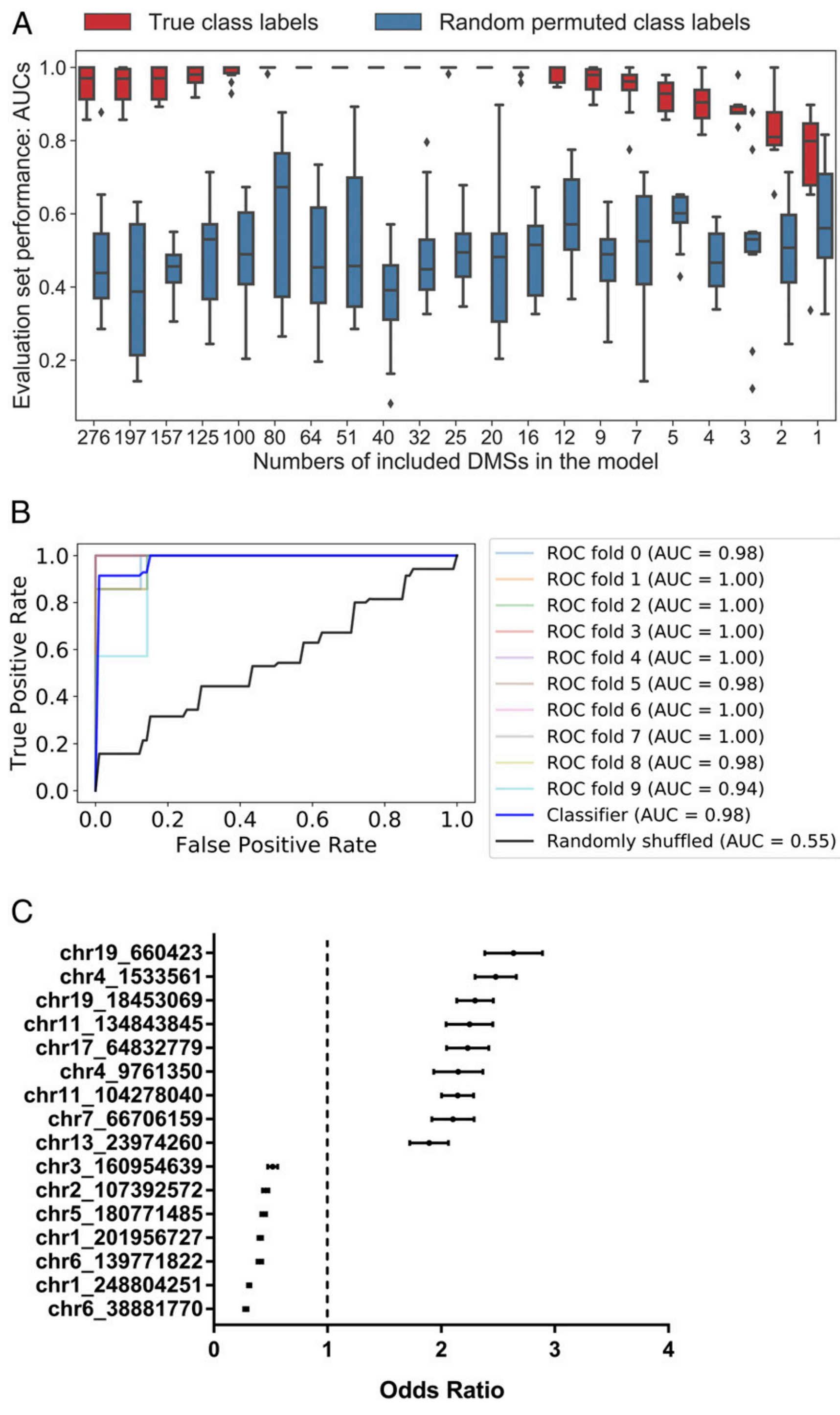

Fig. 2. Specific DMSs prioritize differential APMB vs. ARMB signatures in a classification model. (*A*) Evaluation set performance of the logistic regression classifiers, in order of decreasing number of DMSs used in model construction, from left to right (*x* axis). Red box–whisker plots show the quartiles of 10 AUC values generated from 10-fold of leave one class out cross-validations, and blue box–whisker plots depict the performance based on permuted class labels to represent the random background distribution. (*B*) ROC curve of the logistic regression model that uses the DNA methylation levels of the top 16-ranked CpG sites to distinguish APMB and ARMB samples. (*C*) Plots depicting the mean with 95% CI of odds ratio for the top 16 DMSs in the model shown in *B*.

sites of its proximal genes were determined (*SI Appendix*, Table S2). We found that DMSs are significantly enriched 5 to 50 kb upstream and >50 kb downstream relative to transcriptional start sites (TSSs) and largely depleted between 5 kb upstream and 5 kb downstream to the TSS (Fig. 3*A*). Another view of the genomic distribution for DMSs revealed enrichment of DMSs at introns and intergenic regions, with significant depletion 1 to 10 kb upstream of TSS, 5′ untranslated region (UTR), and coding sequence exon regions (Fig. 3*B*). Together, these results indicate that the differential DMSs in APMB vs. ARMB are enriched at regions distal to promoters.

DMSs Localize to Regulatory Regions Containing Relevant Transcription Factor Binding Sites. To further explore the link between differential methylation and regulation of gene expression, we analyzed

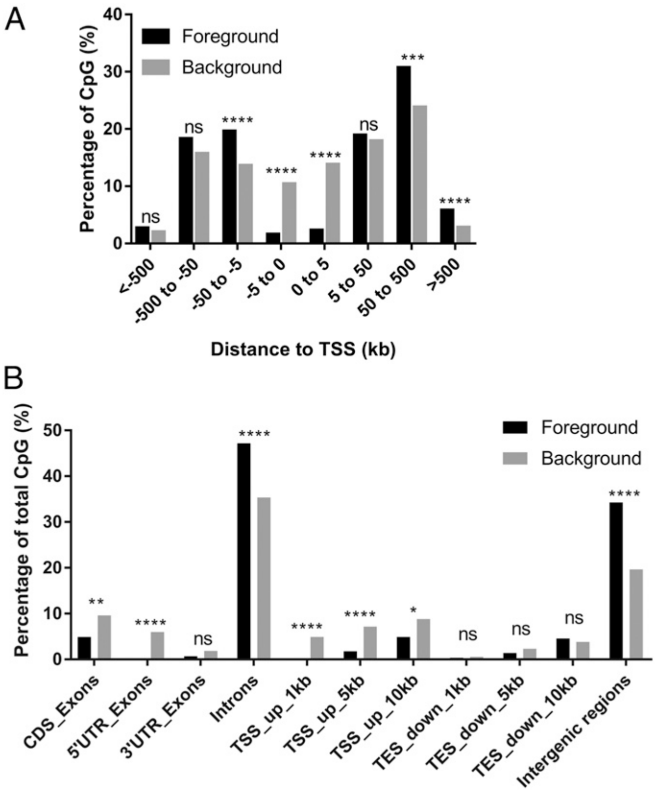

Fig. 3. DMSs are enriched in introns and intergenic regions. (*A*) Distance of DMSs (foreground) to the TSSs of the proximal genes. Background was defined by total detected CpG sites excluding DMS sites. The statistics were calculated using χ^2 test with Yates' correction. (*B*) DMS locations in genomic regions. (CDS, coding sequence; UTR, untranslated region; TSS, transcriptional start site; TES, transcriptional end site.) The statistics were calculated using Fisher's exact test. (ns, not significant; $^*P < 0.05$; $^{**}P < 0.01$; $^{***}P < 0.001$; $^{****}P < 0.0001$.)

DMS enrichment in transcription factor binding sites. To this end, we used Locus Overlap Analysis (LOLA) (22) to comparatively overlay the DMS locations with experimentally validated chromatin immunoprecipitation sequencing (ChIP-seq) peaks (*SI Appendix*, Table S4). Significant overlap ($P < 0.05$) was observed between the DMS and specific transcription factor binding sites, including the signal transducer/activator of transcription 1 (STAT1), histone acetyltransferase p300 (p300), CCAAT enhancer binding protein-β (C/EBPβ), and glucocorticoid receptor (GR) (Fig. 4*A*).

Since DNA hypomethylation at a transcription factor binding motif is often associated with increased transcription factor binding and gene expression, we investigated methylation levels of DMS with potential transcription factor binding sites. We calculated the delta methylation levels of DMS with at least one overlap with transcription factor binding site ($n = 16$) and annotated this mapping with transcription factor binding enrichment (Fig. 4*B*). This analysis revealed 11 DMSs with hypomethylation in APMB, and 5 DMSs having hypomethylation in ARMB. Nine of the 11 DMSs hypomethylated in APMB overlapped with transcription factor binding sites C/EBPβ, and 3 of 11 overlapped with those for STAT1. These genes are well-established regulators of immune and antimicrobial host defense responses (23, 24). Similarly, all five DMSs with hypomethylation in ARMB overlapped with transcription factor binding sites for GR, known to regulate stress responses to sepsis (25, 26). p300 functions as a coactivator by interacting with several transcription factors including GR to increase gene expression (27). The distributions of DNA methylation in each cohort of patients are summarized in Fig. 4 *C* and *D*, segregated by directionality of change in methylation levels relative to APMB vs. ARMB.

For the 11 DMSs with reduced methylation levels in APMB, we observed a populational shift, suggesting overall increased immunologic functions orchestrated by the binding of C/EBPβ and STAT1 in APMB patients (Fig. 4*C*). For the five DMSs having hypomethylation in ARMB, the individual DNA methylation levels ranged from 0 to 100% among SAB patients, demonstrating high methylation variability at the GR and p300 transcription factor binding sites. Specifically, we observed a shift toward M-shaped distributions in ARMB, resulting from a larger subgroup (24 to 29%) of ARMB patients with hypomethylated DMS (Fig. 4*D*). This result suggested that there was a larger subgroup of ARMB patients with immune cells accessible for GR and p300 transcription factor binding. Collectively, these data demonstrate two distinct DNA methylation patterns at transcription factor binding motifs differentiating APMB from ARMB.

Differential Methylation Is Enriched in Myeloid Lineages of APMB vs. ARMB Patients. To investigate whether the 16 transcription factor binding DMSs are located at imputed enhancer regions, we searched for enhancers reported in the GeneHancer database (28). We confirmed a total of six imputed enhancers reported in GeneHancer associated with nine transcription factor binding DMSs (Table 2). Four of 11 DMSs exhibiting hypomethylation in APMB localized at imputed enhancer regions known to regulate SETD6, ADGRG1, and SLC7A5 proteins involved in innate immune cell signal transduction. All five DMSs having hypomethylation in ARMB (two DMSs located at chromosome 19; three DMSs located at chromosome 22) were associated with two enhancers, which regulate lysosome-membrane protein (CTNS) or extracellular matrix protein (FBLN1), respectively.

As transcription factor binding patterns are typically cell-type specific (29, 30), we analyzed whether the 16 transcription factor binding DMSs are enriched in specific cell populations. Methylation data from healthy human adult blood cells were obtained through the Blueprint Human Blood Cell Epigenome project (31). To ensure high-confidence leukocyte-specific DNA methylation data, we included CpG sites with at least 10-read coverage across all 37 leukocyte samples (*SI Appendix*, Table S5) in this analysis (10 of 16 DMSs). All 10 DMSs with validated data quality exhibited hypomethylation in the myeloid lineages as compared with cell types from lymphoid lineage (Fig. 5*A*).

Cell-Type Proportions Estimated from DNA Methylation Differentiate APMB from ARMB. To address the possibility that DNA methylation levels could vary due to changes in cell-type abundance across individuals, analyses were performed to assess cellular composition in blood samples in APMB and ARMB patients. A cell-type deconvolution method was used to estimate cell-type proportions (32–34). This approach obviated potential bias with respect to missing complete blood count data in the study cohort (up to 57%). The DNA methylation-based cell-type decomposition analysis results confirm that estimated cell-type compositions in APMB and ARMB groups had significant differences in relevant cell subsets (multivariate ANOVA, $P = 0.004$). We found significantly higher neutrophils (adjusted P value = 0.003), lower B cells (adjusted P value = 0.026), and lower CD8+ T cells (adjusted P value = 0.02) associated with APMB outcome (Fig. 5 *B* and *C*). Incorporating estimated cell-type composition into the logistic regression model, we obtained average AUC equal to 0.87 (*SI Appendix*, Fig. S3), suggesting that cell-type composition had only a minor effect on improving classification.

TBS-seq Confirmed the Disease-Associated Differential DNA Methylation Signatures. To further validate the DMS identified by RRBS, we carried out TBS-seq (35). A panel of probes was designed to target

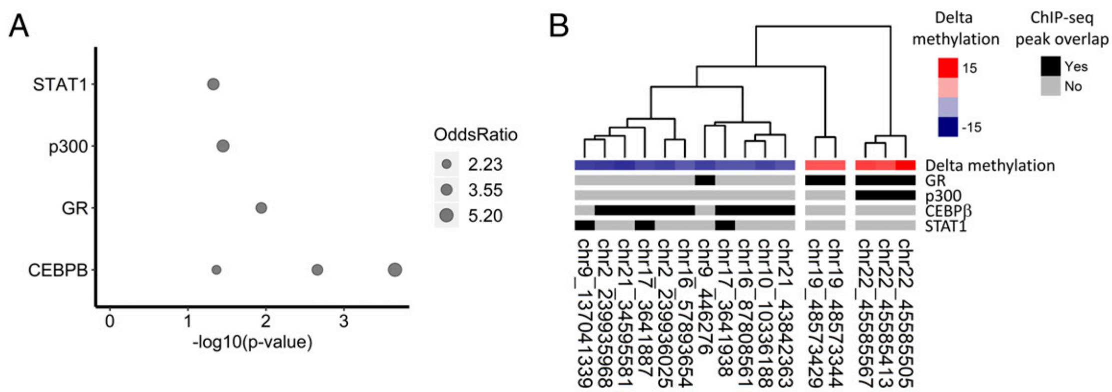

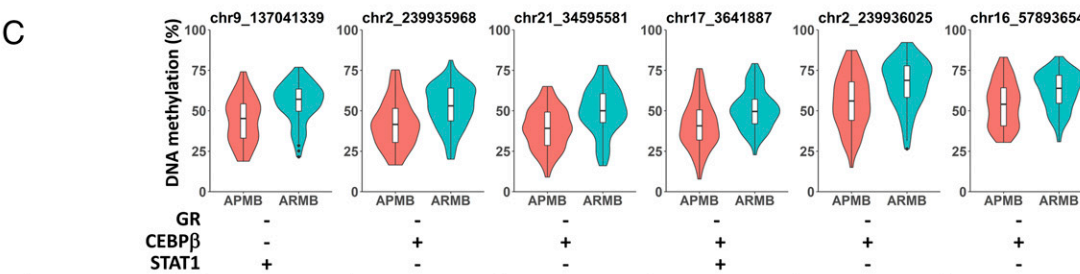

DNA methylation <25%	chr9_137041339	chr2_239935968	chr21_34595581	chr17_3641887	chr2_239936025	chr16_57893654
ARMB (N=72)	1(1)	2(3)	4(6)	1(1)	0(0)	0(0)
APMB (N=70)	7(10)	7(10)	9(13)	9(13)	2(3)	0(0)

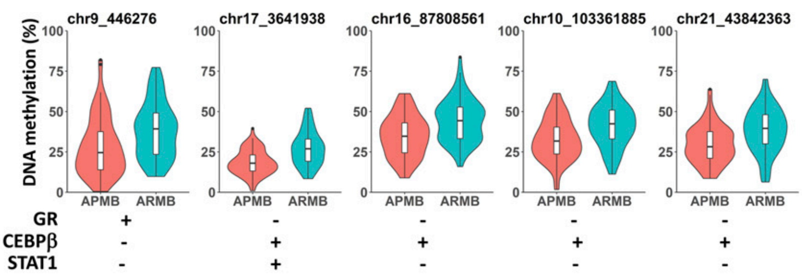

DNA methylation <25%	chr9_446276	chr17_3641938	chr16_87808561	chr10_103361885	chr21_43842363
ARMB (N=72)	21(29)	33(46)	3(4)	10(14)	13(18)
APMB (N=70)	37(53)	55(79)	18(26)	20(29)	25(36)

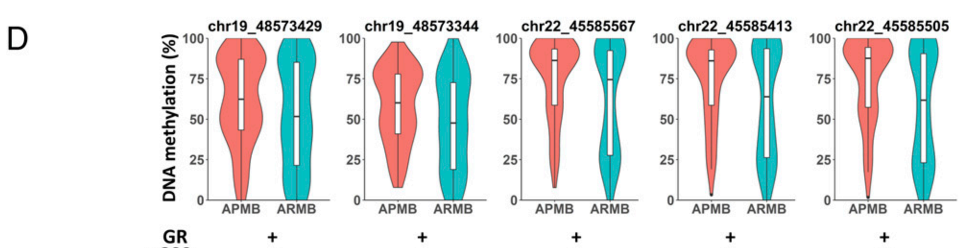

DNA methylation <25%	chr19_48573429	chr19_48573344	chr22_45585567	chr22_45585413	chr22_45585505
ARMB (N=72)	19 (26)	21 (29)	17 (24)	17 (24)	20 (28)
APMB (N=70)	9 (13)	7 (10)	4 (6)	5 (7)	6 (9)

Fig. 4. DMSs localize to regulatory regions containing transcription factor binding sites. (*A*) LOLA region set enrichment analysis displays the significant associations ($P < 0.05$) between transcription factor binding sites (*y* axis) and DMS. The area of points represents the magnitude of odds ratio (a value of zero is mapped to a size of zero). (*B*) The heat map shows the overlap of DMS with transcription factor binding sites that LOLA analysis of the ChIP-seq datasets identified as enriched. Columns were arranged by hierarchical clustering with Ward.D2 method based on the methylation profiles of the 16 transcription factor binding DMSs across all SAB patients. (*C* and *D*) Violin plots of methylation levels for (*C*) DMS with reduced methylation in APMB and (*D*) DMS with reduced methylation in ARMB. Overlap with transcription factor binding site shown as + for yes and − for no. Frequency of patients with hypomethylated DMS (<25% methylation level) in APMB and ARMB shown as number (percentage).

Table 2. DMSs localizing to enhancers as identified from the GeneHancer databank

DMS	GH identifier	Enhancer score	GH sources	No. of putative transcription factor binding sites	Putative gene targets
chr16_87808561	GH16J087805	2	FANTOM5, Ensembl, ENCODE, dbSUPER	171	8 genes (ENSG00000260177, SLC7A5, LOC101928659, CTU2, ZC3H18, ZCCHC14, RNF166, MIR6775)
chr16_57893654	GH16J057891	1.5	FANTOM5, ENCODE, dbSUPER	142	13 genes (RSPRY1, ADGRG3, CSNK2A2, SETD6, KIFC3, LOC388282, CNGB1, ADGRG1, CNOT1, CFAP20, ZNF319, GC16P057890, GC16P057897)
chr19_48573344, chr19_48573429	GH19J048572	1.4	Ensembl, ENCODE, dbSUPER	121	3 genes (SULT2B1, DKKL1, SPACA4)
chr17_3641938	GH17J003639	1	ENCODE	108	3 genes (CTNS, TAX1BP3, LOC105371493)
chr21_34595581	GH21J034589	0.9	ENCODE, dbSUPER	20	7 genes (RCAN1, KCNE1, FAM243A, MRPS6, GC21M034577, GC21M034614, GC21M034615)
chr22_45585413, chr22_45585505, chr22_45585567	GH22J045584	0.8	ENCODE, dbSUPER	9	6 genes (LINC01589, PIR61892, GC22M045121, GC22M045550, FBLN1, GC22P045074)

GH, GeneHancer; FANTOM5, Funational annotation of the mammalian genome project; Ensembl, Ensembl gene annotation; dbSUPER, Database of super-enhancers,

the DMS and DMR identified by RRBS (*SI Appendix*, Table S6). Both DNA methylation and genetic data were computed from the bisulfite converted reads aligned to the genome. The intersecting CpG methylation data generated using TBS-seq showed significant correlation between the two techniques (*SI Appendix*, Fig. S5*B*) and with the MRSA disease-associated DMS detected by RRBS (Fig. 6*A*). Overall, there was excellent concordance between outcomes of the two methods. As an example, all three of the DMSs positively associated with APMB by RRBS (Fig. 2*C*) for which probes could be designed were confirmed by TBS-seq (Fig. 6*B*). Furthermore, all seven hypomethylated DMSs (Fig. 4*C*) and five hypermethylated DMSs associated with transcription factor binding for GR, C/EBPβ, and/or STAT1 (Fig. 4*D*) were confirmed in the TBS-seq data (Fig. 6*C*). The performance of the classification of the 121 DMSs overlapping between TBS-seq and RRBS was evaluated by a 10-fold cross-validation. The average classification accuracy resulted in an AUC of 0.90 for TBS-seq (Fig. 6*D*) and 0.93 for RRBS (Fig. 6*E*), confirming that these DNA methylation signatures differentiate APMB from ARMB.

To determine if the disease-associated DMRs overlap with genetic polymorphisms that may be attributable to disease phenotype, we analyzed the sequence of the AA, AG, and GG alleles based on reads mapping to the forward strand and CC, CT, and TT alleles based on reads mapping to the reverse strand. Genotypes were determined for the majority of alleles in our target regions by correlating the observed counts with the expected counts for each allele combination (*Materials and Methods*). Fisher's exact test was computed for each single-nucleotide polymorphism (SNP) genotype, and the adjusted P values were calculated based on the false discovery rate (FDR) methods. Of the 774 SNP genotypes that were identified within the targeted regions, no significant statistical associations were found between APMB/ARMB outcomes (*SI Appendix*, Table S7). This pattern of results signifies that epigenetic, not genetic, determinants accounted for these distinct outcomes of MRSA bacteremia.

Discussion

The current study compared DNA methylomes in whole-blood leukocytes from patients with APMB and ARMB to assess if differential methylation signatures exist and if so, whether such epigenetic signatures associate with relevant immune functions. Key findings revealed significant differences of DMSs in APMB vs. ARMB patients and localized predominant signals proximate to transcription factor binding sites of genes known to influence immune functions. These data strongly support our hypothesis that differential methylation in circulating immune cells may shape protective vs. nonprotective responses during early stages of MRSA bacteremia that affect ensuing APMB vs. ARMB outcomes. These insights serve as a proof of concept that DNA methylation profiles within host immune cells may aid in APMB classification or predict therapeutic outcomes.

Our findings emphasize that epigenetic regulation correlates with protective immunity in response to *S. aureus* infection. Importantly, DMSs identified were enriched at gene enhancers known to regulate transcription factor binding sites and control cell type-specific gene activation or repression (36, 37). DNA hypomethylation at gene enhancers can switch such enhancers to an active state (38), resulting in enhanced transcription factor binding and gene expression. Our results demonstrated two groups of transcription factor binding patterns associated with significant differences in leukocyte methylation associated with APMB. In turn, these patterns offer plausible mechanistic roles of these transcription factors in the development of APMB.

First, our data support the concept of emergency granulopoiesis in APMB. We observed 11 DMSs exhibiting hypomethylation in APMB, 9 of which were bound by *C/EBPβ*. The C/EBPβ protein is a key transcription factor in emergency granulopoiesis, rapidly mobilizing bone marrow granulocyte progenitors during severe systemic infection (23, 39). Additionally, C/EBPβ amplifies emergency granulopoiesis by inducing FancC expression in infection (39). In support of this finding, up-regulation of C/EBPβ transcripts is observed in granulocyte progenitors, and C/EBPβ-deficient progenitors have impaired pathogen-induced granulopoiesis in vitro and in vivo (23). Because immature neutrophils (e.g., band cells) may be ineffective at killing *S. aureus* or may promote harmful nonspecific inflammation, ostensibly they may be adverse in resolving SAB, facilitating persistence. Further studies are needed to determine if APMB patients have increased release of early granulocyte precursors during MRSA bacteremia.

Second, the polarization of CD4+ T helper (Th) cells during early stages of SAB may be critical in determining subsequent

https://doi.org/10.1073/pnas.2000663118

APMB from ARMB outcomes. For example, Th17 responses during *S. aureus* infection are important for protective immunity, as the cytokines interleukin-1 (IL-1) and IL-17 mediate neutrophil recruitment and activation necessary for bacterial clearance (40, 41). However, the present results in APMB patients reveal hypomethylation at transcription binding sites for STAT1 (Th1 promoting), not STAT3 (Th17 promoting). Importantly, STAT1 induces gamma interferon signaling during infections (42, 43) but counterregulates Th17 polarization (44). Incorporating these findings, we posit that APMB may result in part from a profusive epigenetic activation of STAT1, which in turn, suppresses protective antistaphylococcal immune response mechanisms induced via Th17 pathways. This phenomenon is also consistent with inadequate neutrophil-mediated protection associated with emergency granulopoiesis.

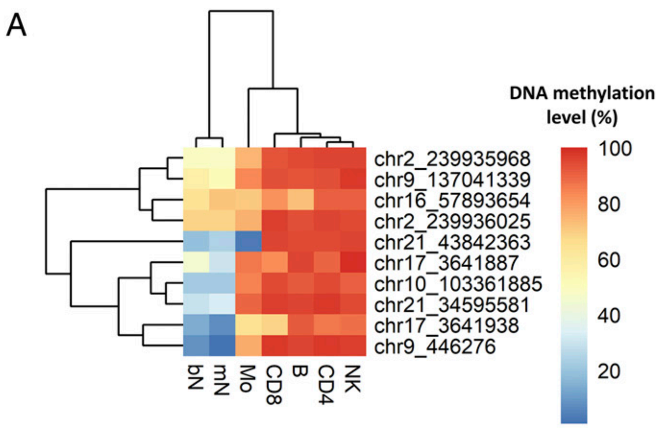

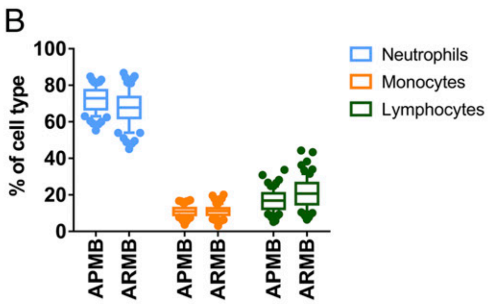

Estimated Percentages [%]	APMB (N=70)	ARMB (N=72)	FDR-adjusted anova p-value
Neutrophil	71.91 ± 6.75	67.60 ± 9.36	0.003
Monocyte	11.05 ± 2.95	11.13 ± 3.31	0.879
Lymphocyte	17.04 ± 5.73	21.27 ± 8.17	0.002

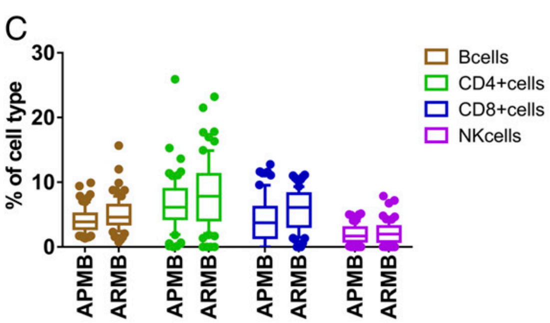

Estimated Percentages [%]	APMB (N=70)	ARMB (N=72)	FDR-adjusted anova p-value
B cells	4.15 ± 1.86	5.08 ± 2.50	0.026
CD4+ T cells	6.68 ± 4.00	8.22 ± 5.02	0.061
CD8+ T cells	4.26 ± 3.40	5.79 ± 3.02	0.020
NK cells	1.95 ± 1.42	2.18 ± 1.70	0.389

Fig. 5. Cell-type proportions estimated from DNA methylation differentiating APMB from ARMB. (*A*) Cell type-specific methylation levels obtained from Blueprint for the transcription factor binding DMS. B, B cell; bN, band neutrophil; mN, mature neutrophil; Mo, monocyte; NK, natural killer cell. (*B* and *C*) Box plots of proportions of each cell type within APMB/ARMB groups. The FDR-corrected ANOVA test within each cell type was used, and the adjusted *P* values smaller than 0.05 are highlighted in red. (*B*) The proportions of estimated neutrophils, lymphocytes (combining the estimated proportions of B, CD4+ T, CD8+ T, and NK cells), and Mos within APMB/ARMB groups. (*C*) The proportions of estimated lymphocytes (including B, CD4+ T, CD8+ T, and NK cells).

Third, we identified five GR transcription factor binding sites to be hypomethylated in the ARMB patient cohort. Glucocorticoid-mediated homeostasis is important in the stress response to sepsis by modulating excessive proinflammatory activities through inactive activator protein-1 (AP-1) or nuclear factor kappa B (NF-κB) (25). In this respect, activated GR can directly engage its coactivator p300 to regulate GR signaling. Thus, our data suggest a mechanistic link between GR–p300 signaling and ARMB, in which modulated immune responses facilitate bacteremia resolution. While glucocorticoids are often used in therapy of infections involving the central nervous system, uncertainty remains about their use as adjuvant therapy for bacteremia and sepsis (45). Previous studies suggest that distinct GR expression levels in septic patients may contribute to treatment responsiveness (46, 47). Our results showing diverse DNA methylation levels in GR transcriptional binding sites among SAB patients may offer further insights into patient responses to glucocorticoid therapy through epigenetic regulation of glucocorticoid response.

Finally, current data reveal important insights into diversity of biological responsiveness to *S. aureus* infection based on interindividual variance of methylomic signatures. We recently identified a genetic polymorphism located in the DNMT3A gene (g.25498283A > C genotype), which correlates with resolving MRSA bacteremia outcomes, potentially via hypermethylation gene regulation resulting in reduced IL-10 levels (11). Furthermore, circulating immune cell-type profiles are dynamic and may also influence differences in methylation patterns of immune cells in APMB vs. ARMB. For example, DNA methylation in human hematopoietic development is affected by adaptive changes in lineage of specific immune cell subsets (29, 30). Our current results highlighted that the majority of transcription factor binding DMSs were demethylated in neutrophils. Therefore, this observation suggests that overall differences in methylation result from a higher proportion of DMSs in circulating neutrophils or band neutrophils in APMB compared with ARMB. This conclusion is also highly consistent with our present findings regarding *C/EBPβ* and *STAT1* methylation signatures with respect to neutrophils.

It is important to note that differential methylation using RRBS analysis can potentially be confounded by the presence of single-nucleotide variants in cis. To validate our initial RRBS findings, TBS-seq was performed. Findings from TBS-seq strongly supported the interpretation that disease-associated interindividual differences were only driven by changes in DNA methylation levels and not SNPs found in our target regions. Notwithstanding this key finding, it should also be understood that variation in gene sequence can influence persistent vs. resolving MRSA bacteremia outcomes (11). Thus, it is plausible that both epigenetic and genetic signatures are associated with APMB/ARMB outcomes in MRSA bacteremia.

Initial results raised the possibility that cellular composition profiles could be influencing APMB classification. Importantly, methylation variability may result from several potential factors, including 1) direct changes of methylation levels at a regulatory element in one or more specific cell type(s) or 2) altered cell-type compositions indirectly impacting methylation levels at a cell type-specific regulatory element (29, 30). To explicitly

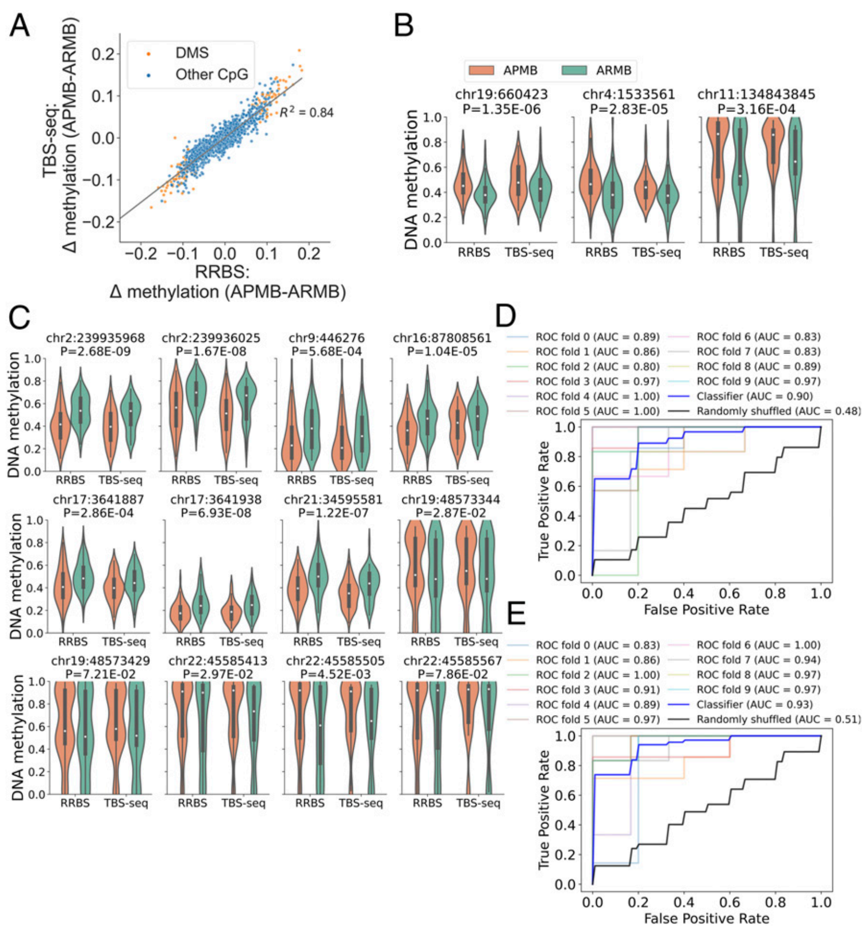

Fig. 6. TBS-seq confirmed the disease-associated differential DNA methylation signatures. (*A*) Scatterplots of the delta methylation (APMB–ARMB) in RRBS (*x* axis) and in TBS-seq (*y* axis). (*B* and *C*) Violin plots of methylation levels in RRBS and TBS-seq for (*B*) top-ranked DMSs reported in Fig. 2 and (*C*) transcription factor binding DMSs reported in Fig. 4. Two-way ANOVA was used to determine the disease associated (*P* value shown). (*D* and *E*) ROC curves of the logistic regression model that uses the DNA methylation levels of 121 detected DMSs from (*D*) TBS-seq and (*E*) RRBS.

segregate these two potential sources of variability, obtaining cell composition information is required. Given the limitation that complete blood counts were not available from every patient studied, we employed a method to correct methylation profile data based on potential cell-type composition. We found that the cell-type abundances were similar between the persistent and resolving groups. However, some of these differences achieved statistical significance for relevant immune cell subsets. Moreover, we demonstrated that our classification model, which has an AUC = 0.85 without accounting for cell-type composition, is only modestly improved by explicitly including inferred cell-type abundances as covariates. These results support the conclusion that methylation differences, comprising both disease- and cell type-associated features, may be useful to develop an agnostic algorithm to inform or predict clinical outcomes in MRSA bacteremia patients.

Whether the host, pathogen, or a combination of the two drives differential methylation is the key question that remains to be determined. Pathogens may drive alterations of DNA methylation in host immune cells, supporting the emerging concept of innate immune memory (48–50). For example, *Mycobacterium tuberculosis* (15) and *Helicobacter pylori* (51) have been reported to subvert host DNA epigenetics through ten-eleven translocation (TET) enzyme family and inducing de novo DNA methylation. One recent observation further supported this concept that DNA demethylation was induced after *M. tuberculosis* infection (52). Thus, it is possible that the host epigenetic changes identified in the current study were driven by prior episodes of infection, *S. aureus* or otherwise.

It is also important to note the limitations of the current investigation. First, this study was not designed to explicitly determine APMB vs. ARMB outcome-associated SNPs, and it is challenging to accurately identify the heterozygous single-nucleotide variants (SNVs) from partially C to T converted sequences in the bisulfite conversion conditions. Second, our annotation analyses were limited by the scope of data available in the University of California Santa Cruz (UCSC) genome browser, the Encyclopedia of DNA Elements (ENCODE), and the CODEX databases, which are largely generated from uninfected human cell lines. Third, the current SAB classification model has not been evaluated using an external validation cohort. However, a principal goal of this study was to compare RRBS sequencing data and methylation characteristics in SAB patients experiencing APMB vs. ARMB outcomes. Thus, we demonstrate findings not available from any prior investigation to our knowledge, namely genome-wide methylation signatures associated with persistent outcomes in MRSA bacteremia. Fourth, precise impact of the methylation patterns uncovered in this study requires future investigation. While hypomethylation is generally felt to promote gene expression, recent studies have challenged this view. For example, Pacis et al. (52) suggest that gain or loss of methylation may be associated with increased transcriptional activity, particularly at nonpromoter, enhancer regions. Finally, the current study focused on patients with clinically confirmed MRSA bacteremia receiving appropriate vancomycin therapy over a 5-d course.

Whether the specific epigenetic pattern differences are the same in such patients treated with other antibiotic regimens remains to be determined. In this respect, the current study establishes an important reference point. Thus, our ongoing efforts are focused on determining the impact of methylation status on expression of key immune system genes and their expression in MRSA infection and beyond.

In summary, the current findings support a proof of principle that DNA methylation signatures in host immune effectors can differentiate persistent vs. resolving outcomes in MRSA infection. Moreover, specific DMSs identified correspond to immune cell regulatory functions of direct and established relevance to host defense against *S. aureus*. The fact that targeted methods validated general methods suggests that targeted methods may be readily developed into much more expedient and practical assays for rapid assessment of likelihood for persistent MRSA bacteremia outcomes. In turn, such knowledge could guide interventions that minimize likelihood for such adverse outcomes. These concepts could also logically extend to many other types of infections. The implications for future studies include testing the predictive value of targeted CpG sites for APMB detection, as well as studying in vivo how DNA methylation correlates with gene expression in specific cell subsets and in context of antiinfective therapy.

Materials and Methods

Case Selection. All human studies were conducted in accordance with Good Clinical Practice and Human Subjects Research as approved by the Duke University Medical Center (DUMC) Institutional Review Board. SAB cases were evaluated and consented for enrollment in the *S. aureus* Bacteremia Group (SABG) biorepository at DUMC. Cases for the current study were carefully selected based on the following inclusion criteria: laboratory-confirmed MRSA bacteremia, received appropriate vancomycin therapy, and enrolled in the SABG study between 2007 and 2017 (to ensure contemporary medical practices). APMB was defined in patients who had continuous MRSA-positive blood cultures for at least 5 d after vancomycin antibiotic treatment (11); ARMB patients had initial blood cultures that were positive for MRSA, but the subsequent blood cultures became negative. Thus, epigenetic methylome patterns in this study focused on circulating host immune cells proximate to the time of SAB diagnosis. Stratified propensity scoring was used to match the demographic and clinical variables for selection of APMB vs. ARMB cases, including race, sex, age, dialysis, diabetes diagnosis, and/or presence of indwelling device (artificial heart valve, peritoneal dialysis port, central venous/arterial catheter, or left ventricular assist device) and vancomycin treatment. This case-controlled study was based on a total of 142 SAB samples (70 APMBs and 72 ARMBs) with matched criteria and qualified DNA quality control. Details of clinical characteristics of the study cohort are presented in Table 1.

RRBS. RRBS libraries were prepared as described previously (53) and sequenced by University of California, Los Angeles, Broad Stem Cell Research Center (BSCRC) sequencing core. The data were subjected to a quality control step using FastQC (version 0.11.7) (54). Sequencing data were trimmed to remove the adaptors and the terminal CG nucleotides using the trimmomatic software (version 0.38) (55). The reads were aligned to the human genome GRCh38/hg38 (release 93, downloaded from Ensembl), and DNA methylation levels were determined using the BS-Seeker2 pipeline (56). Data were filtered to include the autosomal CpG sites with at least 15-read coverage across all samples, and the potential confounding factors, including batch, race, and sex, were accounted for by using an empirical Bayesian framework, as implemented in the ComBat function of R package SVA as in previous reports (30, 57). Details are in *SI Appendix*.

TBS-seq. A total of 1,117 probes were designed by Integrated DNA Technologies based on the coordinates of the DMSs we discovered using RRBS data. The libraries were prepared as described in *SI Appendix*. Data were preprocessed with FastQC (version 0.11.8) and cutadapt (version 2.10) to remove the adapter sequences. Trimmed reads were aligned against the GRCh38 genome using BSBolt (58) according to the pipeline described in ref. 35. Methylation was called on aligned reads after PCR duplicates removal, and the DNA methylation matrix was assembled using the common CpG sites covered by at least 20 reads across all samples. A total of 3,614 intersecting CpGs detected from both RRBS and TBS-seq were collected, which included the 121 DMSs and five DMRs reported from RRBS. The correlation between data generated from the two methods was computed, and the two-factor ANOVA was used to determine the statistical difference among factors including the disease outcomes and techniques. The genotype data were generated as described in *SI Appendix*. Fisher's exact test was used to determine the association between SNP genotypes and APMB/ARMB outcomes.

Classification of Patients. Logistic regression was used to build a classifier using the Python package, scikit-learn version 0.21.2. A regularization method elastic net (18) was incorporated in the classification model to build a generalizable classifier and reduce model overfitting. All RRBS-detected 749,212 CpGs were included in the optimization phase using both precision and recall score for the model evaluation. Then, the classifiers were trained and tested using a 10-fold cross-validation strategy. ROCs were used to estimate the sensitivity and specificity of the APMB classification method. The AUC was calculated for each ROC to evaluate the accuracy of APMB classification.

CpG Clustering and Identification of DMSs and Regions. The clustered CpG regions were generated based on the dynamic fragmentation strategy in CGmapTools (20) (with the following parameters: maximal distance between two adjacent CpGs, s = 100 bp; maximal fragment size, S = 1,000 bp; minimal CpG number in one fragment, $n = 2$) The matrix of the single CpG site or the clustered CpG region was then used to calculate the differential methylation sites using the methylkit package in R (19). The cutoff of q value < 0.01 and methylation difference larger than 10% were used to define DMSs.

Genomic Landscape of DMS. The DMS distances to TSSs were determined using the Genomic Regions Enrichment of Annotations Tool (http://great.stanford.edu/public/html/) (details are in *SI Appendix*), and the genomic distribution was determined by using the script of read_distribution.py file with the reference file (hg38_RefSeq.bed) in the software package, RSeQC (version 2.6.4). LOLA (22) was to identify significant overlaps of DMS regions with transcription factor binding sites based on ChIP-seq datasets obtained from ENCODE (59) and CODEX (60) databases. The Fisher's exact test was used with a significance threshold of 0.05 on FDR-adjusted P values. The whole-enrichment results together with their original and curated annotations are presented in *SI Appendix*, Table S4.

Cell Type-Specific DNA Methylation. The DNA methylation data (data type: methylation signal) for specific leukocytes were downloaded from Blueprint Epigenome Project DCC portal (31). The analysis was performed using the selected 37 Blueprint Bisulfite-Seq experiments (*SI Appendix*, Table S5). The low-coverage CpG sites (<10-read coverage) in each sample were first excluded, and intersection against the genome-wide locations of autosomal CpG sites was performed, resulting in a total of 4,861,556 CpG sites. The details are in *SI Appendix*.

Data Availability. The DNA methylation sequence data reported in this paper have been deposited into the Gene Expression Omnibus (accession no. GSE150144). All other data, associated protocols, and materials used in this work are described in the paper.

ACKNOWLEDGMENTS. These studies were supported in part by NIH Grants U01-AI124319 (to M.R.Y.), R01-AI068804 (to V.G.F.), R33-AI111661 (to M.R.Y.), U01-AI124319 (to E.F.R.), and U19AI128913 (to E.F.R.).

1. S. Y. Tong, J. S. Davis, E. Eichenberger, T. L. Holland, V. G. Fowler Jr, *Staphylococcus aureus* infections: Epidemiology, pathophysiology, clinical manifestations, and management. *Clin. Microbiol. Rev.* **28**, 603–661 (2015).
2. V. G. Fowler Jr *et al*., Persistent bacteremia due to methicillin-resistant *Staphylococcus aureus* infection is associated with agr dysfunction and low-level in vitro resistance to thrombin-induced platelet microbicidal protein. *J. Infect. Dis.* **190**, 1140–1149 (2004).
3. G. Sakoulas *et al*., Reduced susceptibility of *Staphylococcus aureus* to vancomycin and platelet microbicidal protein correlates with defective autolysis and loss of accessory gene regulator (agr) function. *Antimicrob. Agents Chemother.* **49**, 2687–2692 (2005).
4. Y. Q. Xiong *et al*., Phenotypic and genotypic characteristics of persistent methicillin-resistant *Staphylococcus aureus* bacteremia in vitro and in an experimental endocarditis model. *J. Infect. Dis.* **199**, 201–208 (2009).
5. N. A. Turner *et al*., Methicillin-resistant *Staphylococcus aureus*: An overview of basic and clinical research. *Nat. Rev. Microbiol.* **17**, 203–218 (2019).
6. A. Harms, E. Maisonneuve, K. Gerdes, Mechanisms of bacterial persistence during stress and antibiotic exposure. *Science* **354**, aaf4268 (2016).
7. J. H. Jiang *et al*., Antibiotic resistance and host immune evasion in *Staphylococcus aureus* mediated by a metabolic adaptation. *Proc. Natl. Acad. Sci. U.S.A.* **116**, 3722–3727 (2019).

8. A. Di Pietro, K. L. Good-Jacobson, Disrupting the code: Epigenetic dysregulation of lymphocyte function during infectious disease and lymphoma development. *J. Immunol.* **201**, 1109–1118 (2018).
9. L. C. Chan *et al*., Innate immune memory contributes to host defense against recurrent skin and skin structure infections caused by methicillin-resistant *Staphylococcus aureus*. *Infect. Immun.* **85**, e00876-16 (2017).
10. L. C. Chan *et al*.; MRSA Systems Immunobiology Group, Protective immunity in recurrent *Staphylococcus aureus* infection reflects localized immune signatures and macrophage-conferred memory. *Proc. Natl. Acad. Sci. U.S.A.* **115**, E11111–E11119 (2018).
11. F. Mba Medie *et al*.; MRSA Systems Immunobiology Group, Genetic variation of DNA methyltransferase-3A contributes to protection against persistent MRSA bacteremia in patients. *Proc. Natl. Acad. Sci. U.S.A.* **116**, 20087–20096 (2019).
12. B. Suarez-Alvarez, R. M. Rodriguez, M. F. Fraga, C. López-Larrea, DNA methylation: A promising landscape for immune system-related diseases. *Trends Genet.* **28**, 506–514 (2012).
13. N. Bhutani, D. M. Burns, H. M. Blau, DNA demethylation dynamics. *Cell* **146**, 866–872 (2011).
14. H. R. Moinova *et al*., Identifying DNA methylation biomarkers for non-endoscopic detection of Barrett's esophagus. *Sci. Transl. Med.* **10**, eaao5848 (2018).
15. A. Pacis *et al*., Bacterial infection remodels the DNA methylation landscape of human dendritic cells. *Genome Res.* **25**, 1801–1811 (2015).
16. S. H. Sinclair, S. Yegnasubramanian, J. S. Dumler, Global DNA methylation changes and differential gene expression in *Anaplasma phagocytophilum*-infected human neutrophils. *Clin. Epigenetics* **7**, 77 (2015).
17. Y. Michigami *et al*., Long-term effects of *H. pylori* eradication on epigenetic alterations related to gastric carcinogenesis. *Sci. Rep.* **8**, 14369 (2018).
18. H. Zou, T. Hastie, Regularization and variable selection via the elastic net. *J. R. Stat. Soc. B* **67**, 301–320 (2005).
19. A. Akalin *et al*., methylKit: A comprehensive R package for the analysis of genome-wide DNA methylation profiles. *Genome Biol.* **13**, R87 (2012).
20. W. Guo *et al*., CGmapTools improves the precision of heterozygous SNV calls and supports allele-specific methylation detection and visualization in bisulfite-sequencing data. *Bioinformatics* **34**, 381–387 (2018).
21. I. Guyon, J. Weston, S. Barnhill, V. Vapnik, Gene selection for cancer classification using support vector machines. *Mach. Learn.* **46**, 389–422 (2002).
22. N. C. Sheffield, C. Bock, LOLA: Enrichment analysis for genomic region sets and regulatory elements in R and bioconductor. *Bioinformatics* **32**, 587–589 (2016).
23. H. Hirai *et al*., C/EBPbeta is required for 'emergency' granulopoiesis. *Nat. Immunol.* **7**, 732–739 (2006).
24. F. B. Sow *et al*., Role of STAT1, NF-kappaB, and C/EBPbeta in the macrophage transcriptional regulation of hepcidin by mycobacterial infection and IFN-gamma. *J. Leukoc. Biol.* **86**, 1247–1258 (2009).
25. I. M. Adcock, G. Caramori, Cross-talk between pro-inflammatory transcription factors and glucocorticoids. *Immunol. Cell Biol.* **79**, 376–384 (2001).
26. I. M. Adcock, K. Ito, P. J. Barnes, Glucocorticoids: Effects on gene transcription. *Proc. Am. Thorac. Soc.* **1**, 247–254 (2004).
27. K. Dendoncker *et al*., TNF-α inhibits glucocorticoid receptor-induced gene expression by reshaping the GR nuclear cofactor profile. *Proc. Natl. Acad. Sci. U.S.A.* **116**, 12942–12951 (2019).
28. S. Fishilevich *et al*., GeneHancer: Genome-wide integration of enhancers and target genes in GeneCards. *Database (Oxford)* **2017**, bax028 (2017).
29. M. Farlik *et al*., DNA methylation dynamics of human hematopoietic stem cell differentiation. *Cell Stem Cell* **19**, 808–822 (2016).
30. L. Chen *et al*., Genetic drivers of epigenetic and transcriptional variation in human immune cells. *Cell* **167**, 1398–1414.e24 (2016).
31. J. H. Martens, H. G. Stunnenberg, BLUEPRINT: Mapping human blood cell epigenomes. *Haematologica* **98**, 1487–1489 (2013).
32. L. D. Orozco *et al*., Epigenome-wide association in adipose tissue from the METSIM cohort. *Hum. Mol. Genet.* **27**, 2586 (2018).
33. P. Y. Chen *et al*., Prenatal growth patterns and birthweight are associated with differential DNA methylation and gene expression of cardiometabolic risk genes in human placentas: A discovery-based approach. *Reprod. Sci.* **25**, 523–539 (2018).
34. L. Lam *et al*., Epigenetic changes in T-cell and monocyte signatures and production of neurotoxic cytokines in ALS patients. *FASEB J.* **30**, 3461–3473 (2016).
35. M. Morselli *et al*., Targeted bisulfite sequencing for biomarker discovery. *Methods*, 10.1016/j.ymeth.2020.07.006 (2020).
36. S. Heinz, C. E. Romanoski, C. Benner, C. K. Glass, The selection and function of cell type-specific enhancers. *Nat. Rev. Mol. Cell Biol.* **16**, 144–154 (2015).
37. P. L. Clermont, A. Parolia, H. H. Liu, C. D. Helgason, DNA methylation at enhancer regions: Novel avenues for epigenetic biomarker development. *Front. Biosci.* **21**, 430–446 (2016).
38. A. Sharifi-Zarchi *et al*., DNA methylation regulates discrimination of enhancers from promoters through a H3K4me1-H3K4me3 seesaw mechanism. *BMC Genomics* **18**, 964 (2017).
39. C. A. Shah *et al*., Stat3 and CCAAT enhancer-binding protein β (C/ebpβ) activate Fanconi C gene transcription during emergency granulopoiesis. *J. Biol. Chem.* **293**, 3937–3948 (2018).
40. L. S. Miller, J. S. Cho, Immunity against *Staphylococcus aureus* cutaneous infections. *Nat. Rev. Immunol.* **11**, 505–518 (2011).
41. B. M. Bröker, D. Mrochen, V. Péton, The T cell response to *Staphylococcus aureus*. *Pathogens* **5**, 31 (2016).
42. A. Chapgier *et al*., A partial form of recessive STAT1 deficiency in humans. *J. Clin. Invest.* **119**, 1502–1514 (2009).
43. J. Toubiana *et al*.; International STAT1 Gain-of-Function Study Group, Heterozygous STAT1 gain-of-function mutations underlie an unexpectedly broad clinical phenotype. *Blood* **127**, 3154–3164 (2016).
44. A. V. Villarino, E. Gallo, A. K. Abbas, STAT1-activating cytokines limit Th17 responses through both T-bet-dependent and -independent mechanisms. *J. Immunol.* **185**, 6461–6471 (2010).
45. B. Venkatesh *et al*.; ADRENAL Trial Investigators and the Australian–New Zealand Intensive Care Society Clinical Trials Group, Adjunctive glucocorticoid therapy in patients with septic shock. *N. Engl. J. Med.* **378**, 797–808 (2018).
46. E. L. van den Akker *et al*., Glucocorticoid receptor mRNA levels are selectively decreased in neutrophils of children with sepsis. *Intensive Care Med.* **35**, 1247–1254 (2009).
47. K. Vardas *et al*., Increased glucocorticoid receptor expression in sepsis is related to heat shock proteins, cytokines, and cortisol and is associated with increased mortality. *Intensive Care Med. Exp.* **5**, 10 (2017).
48. R. Ostuni *et al*., Latent enhancers activated by stimulation in differentiated cells. *Cell* **152**, 157–171 (2013).
49. J. Quintin, S. C. Cheng, J. W. van der Meer, M. G. Netea, Innate immune memory: Towards a better understanding of host defense mechanisms. *Curr. Opin. Immunol.* **29**, 1–7 (2014).
50. S. Saeed *et al*., Epigenetic programming of monocyte-to-macrophage differentiation and trained innate immunity. *Science* **345**, 1251086 (2014).
51. T. Maekita *et al*., High levels of aberrant DNA methylation in *Helicobacter pylori*-infected gastric mucosae and its possible association with gastric cancer risk. *Clin. Cancer Res.* **12**, 989–995 (2006).
52. A. Pacis *et al*., Gene activation precedes DNA demethylation in response to infection in human dendritic cells. *Proc. Natl. Acad. Sci. U.S.A.* **116**, 6938–6943 (2019).
53. K. Fu *et al*., A temporal transcriptome and methylome in human embryonic stem cell-derived cardiomyocytes identifies novel regulators of early cardiac development. *Epigenetics* **13**, 1013–1026 (2018).
54. R. M. Leggett, R. H. Ramirez-Gonzalez, B. J. Clavijo, D. Waite, R. P. Davey, Sequencing quality assessment tools to enable data-driven informatics for high throughput genomics. *Front. Genet.* **4**, 288 (2013).
55. A. M. Bolger, M. Lohse, B. Usadel, Trimmomatic: A flexible trimmer for Illumina sequence data. *Bioinformatics* **30**, 2114–2120 (2014).
56. W. Guo *et al*., BS-Seeker2: A versatile aligning pipeline for bisulfite sequencing data. *BMC Genomics* **14**, 774 (2013).
57. S. Ecker *et al*.; BLUEPRINT Consortium, Genome-wide analysis of differential transcriptional and epigenetic variability across human immune cell types. *Genome Biol.* **18**, 18 (2017).
58. C. Farrell, M. Thompson, A. Tosevska, A. Oyetunde, M. Pellegrini, BiSulfite bolt: A BiSulfite sequencing analysis platform. https://doi.org/10.1101/2020.10.06.328559 (8 October 2020).
59. J. Harrow *et al*., GENCODE: The reference human genome annotation for the ENCODE project. *Genome Res.* **22**, 1760–1774 (2012).
60. M. Sánchez-Castillo *et al*., CODEX: A next-generation sequencing experiment database for the haematopoietic and embryonic stem cell communities. *Nucleic Acids Res.* **43**, D1117–D1123 (2015).